First insight into human extrahepatic metabolism of flame retardants

Abdallah, Mohamed Abou-Elwafa; Nguyen, Khanh-Hoang; Moehring, Thomas; Harrad, Stuart

DOI:
10.1016/j.chemosphere.2019.04.017

Document Version
Peer reviewed version

Citation for published version (Harvard):
Abdallah, MA-E, Nguyen, K-H, Moehring, T & Harrad, S 2019, 'First insight into human extrahepatic metabolism of flame retardants: biotransformation of EH-TBB and Firemaster-550 components by human skin subcellular fractions', *Chemosphere*, vol. 227, pp. 1-8. https://doi.org/10.1016/j.chemosphere.2019.04.017

First Insight into Human Extrahepatic Metabolism of Flame Retardants: Biotransformation of EH-TBB and Firemaster-550 components by Human Skin Subcellular Fractions

Mohamed Abou-Elwafa Abdallah[1,2], Khanh-Hoang Nguyen[1], Thomas Moehring[3], Stuart Harrad[1]*

[1] School of Geography, Earth and Environmental Sciences, University of Birmingham, Birmingham, B5 2TT, United Kingdom.

[2]Department of Analytical Chemistry, Faculty of Pharmacy, Assiut University, 71526 Assiut, Egypt

[3] Thermo Fisher Scientific (GmbH) Bremen, Hanna-Kunath-Str. 11, 28199 Bremen, Germany

* Corresponding author

E-mail: M.abdallah@bham.ac.uk

Tel.: +44 121 414 5527

Abstract

2-ethylhexyl-2,3,4,5-tetrabromobenzoate (EH-TBB) and a mixture of EH-TBB, Bis(2-ethylhexyl)tetrabromphthalate (BEH-TEBP) and Triphenyl phosphate (TPhP), prepared in a ratio similar to the Firemaster-550™ (FM550) flame retardant formulation, were exposed to human skin subcellular fractions (S9) to evaluate their dermal *in vitro* metabolism for the first time. After 60 mins of incubation, tetrabromobenzoic acid (TBBA) and diphenyl phosphate (DPhP) were identified as the major metabolites of EH-TBB and TPhP, respectively using UPLC-Q-Exactive Orbitrap™-MS analysis. Dermal biotransformation of EH-TBB and TPhP was catalyzed by skin carboxylesterases rather than CYP450 enzymes, while no stable metabolites could be identified for BEH-TEBP. Metabolite formation rates of EH-TBB as individual compound and as a component of FM550 fitted the Michaelis-Menten model, while no steady state could be reached for TPhP under experimental conditions. Estimated maximum metabolic rate (V_{max}) for TBBA formation upon exposure to FM550 was lower than V_{max} for EH-TBB (1.08 and 15.2 pmol min^{-1} mg $protein^{-1}$, respectively). This indicates dermal metabolism would contribute less to the clearance of EH-TBB body burden than hepatic metabolism (V_{max} = 644 pmol min^{-1} mg $protein^{-1}$). Implications for human exposure include EH-TBB accumulation in skin tissue and human exposure to dermal metabolic products, which may have different toxicokinetic and toxicodynamic parameters than parent flame retardants.

Keywords: *Flame retardants; Firemaster 550; EH-TBB; dermal metabolism; human exposure.*

Introduction

2-ethylhexyl-2,3,4,5-tetrabromobenzoate (EH-TBB) is an additive flame retardant produced by Chemtura™ Corporation. It is available in 2 commercial mixtures: Firemaster 550™ (FM550) and Firemaster BZ-54™ (FMBZ-54). In FM550, EH-TBB is mixed with bis(2-ethylhexyl) tetrabromophthalate (BEH-TEBP), triphenyl phosphate (TPhP) and assorted isopropyl triphenylphosphate (ITP) isomers in the ratio: 36% EH-TBB, 14% BEH-TEBP, 18% TPhP and 32% ITPs by weight (Belcher et al., 2014). As additive FRs, EH-TBB and the other components of FM550 may leach out from treated consumer goods and contaminate the environment. They have been detected globally in various environmental matrices including indoor dust,(Carignan et al., 2013; Tao et al., 2016; Hammel et al., 2017) indoor air,(Cequier et al., 2014; Tao et al., 2016) outdoor air,(Ma et al., 2012) chicken eggs,(Zheng et al., 2016) aquatic biota (Strid et al., 2013) and foodstuffs (Xu et al., 2015).

Similar to other emerging FRs, the environmental occurrence of EH-TBB and FM550 components is expected to be mainly in indoor dust. Residential dust in the UK contained median concentrations of EH-TBB and BEH-TEBP at 4 - 23 (median = 5.8) and 80 – 3187 (median = 320) ng/g, respectively (Al-Omran and Harrad, 2016). In the U.S.A., house dust samples from California collected in 2011 showed higher levels of FM550 components than those collected in 2006. Specifically, concentration ranges of EH-TBB and BEH-TEBP in 2011 were 45-5900 (median = 100) and <2-3800 (median = 260) ng/g, while those in 2006 were 4-740 (median = 48) and 36-1900 (median = 140), respectively (Dodson et al., 2012). Extremely high concentrations of EH-TBB and BEH-TEBP were reported in dust from an American gymnasium ranging from 20,800 to 85,600 (median = 28,900) ng/g for EH-TBB and 17,300 to 44,900 (median = 30,000) ng/g for BEH-TEBP (Carignan et al., 2013). This is

of concern due to the potential toxicity of FM550 components to humans and wildlife. Both EH-TBB and BEH-TEBP expressed *in vitro* antiestrogenic and antiandrogenic effects in the yeast estrogen screen and yeast androgen screen assays (reflected in inhibition of β-galactosidase production by the assays), as well as increased oestrogen production in the human H295R steroidogenesis assays (Saunders et al., 2013). By use of primary porcine testicular cells, Mankidy et al. also investigated the effects of EH-TBB and BEH-TEBP on steroidogenesis via different mechanisms; EH-TBB induced the production of cortisol and aldosterone while BEH-TEBP promoted sex hormones synthesis (Mankidy et al., 2014). FM550-administered rats showed many negative health effects e.g. advanced female puberty, weight gain, altered exploratory behaviours and hepatic carboxylesterases activity (Patisaul et al., 2013). FM550 (mainly driven by the TPhP component) was found to bind to human peroxisome proliferator-activated receptor γ (PPARγ1) and subsequently induced PPARγ1 transcription activity. The same study also reported adipogenesis induction in primary mouse bone marrow cultures by FM550 and TPhP (Pillai et al., 2014).

Accidental indoor dust ingestion is reported as a major exposure pathway of humans to EH-TBB, BEH-TBP and TPhP (Besis et al., 2017; Tao et al., 2017). However, the significance of dermal absorption as a pathway of human exposure to halogenated flame retardants via contact with contaminated dust or flame retarded consumer products has been recently highlighted (Abdallah et al., 2016; Frederiksen et al., 2016; Abdallah and Harrad, 2018; Frederiksen et al., 2018). This is of particular relevance to EH-TBB and FM550, which are widely used to flame proof upholstered furniture including childcare products (e.g. car seats and nap mats) (Hammel et al., 2017; Stubbings et al., 2018). A recent study by our research group revealed dermal uptake of some brominated FRs via contact with

upholstered furniture may even exceed exposure via dust ingestion or dietary exposure (Abdallah and Harrad, 2018). Frederiksen et al. reported on the dermal uptake of EH-TBB, BEH-TEBP and TPhP using a human skin *ex vivo* model. Based on the mass balance exercise, dermal biotransformation was suggested for all 3 flame retardants based on their ester chemical structure (Frederiksen et al., 2016; Frederiksen et al., 2018). This is supported by Hopf et al. who found that diethyl hexyl phthalate is completely hydrolysed to monoethyl hexyl phthalate by freshly excised human skin, such that only the metabolites penetrate through the skin to reach systemic circulation (Hopf et al., 2014). While it is reasonable to hypothesize that dermal exposure to EH-TBB and FM550 components via contact with furniture may be substantial, very little is known about human dermal metabolism of these flame retardants. While the hepatic metabolism of these FRs has been studied using various *in vitro* techniques,(Roberts et al., 2012; Van den Eede et al., 2013) the products and role of extrahepatic dermal metabolism of FRs remains largely unknown. Consequently, understanding of the skin biotransformation pathways, rates and products of the esterified flame retardants EH-TBB, BEH-TEBP and TPhP is important for comprehensive risk assessment of these chemicals. Against this backdrop, the current study aims to provide the first insights into the dermal biotransformation of EH-TBB, BEH-TEBP and TPhP using *in vitro* human skin S9 fractions. Specific objectives include: (a) dermal metabolite identification; (b) metabolic rate estimation for EH-TBB as a single compound (FMBZ-54) and in a mixture with BEH-TEBP and TPhP (FM550); and (c) an evaluation of the implications of dermal metabolism for human dermal exposure to the studied flame retardants.

Materials and Methods

Chemicals and Standards

All solvents and reagents used in this study were purchased from Fisher Scientific (Loughborough, UK) and were of HPLC grade or higher. 2-Ethylhexyl-2,3,4,5-tetrabromobenzoate (EH-TBB) and bis(2-ethylhexyl) tetrabromophthalate (BEH-TEBP) for dosing solutions (purity >95%) were obtained as neat standards from AccuStandard, Inc. (New Haven, CT, USA). High-resolution Orbitrap-MS scan of the neat standards revealed no brominated impurities/degradation products. Moreover, no effects on the metabolic activity of the human skin enzymes were observed upon exposure to the EH-TBB and BEH-TEBP standard solutions. High purity standards of EH-TBB, BEH-TEBP, triphenyl phosphate (TPhP), 2-ethylhexyl-2,3,4,5-tetrabromo[$^{13}C_6$]benzoate (^{13}C-EH-TBB), bis(2-ethylhexyl-d_{17})-tetrabromo[$^{13}C_6$]phthalate (^{13}C-BEH-TEBP), tetrabromobenzoic acid (TBBA), ^{13}C-labelled tetrabromobenzoic acid (^{13}C-TBBA) and α-1,2,5,6,9,10-hexabromo[$^{13}C_{12}$]cyclododecane] (^{13}C-α-HBCDD) were purchased from Wellington Laboratories (Guelph, ON, Canada). Triphenyl phosphate-d_{15} (TPhP-d_{15}) and diphenyl phosphate (DPhP) were purchased from Sigma Aldrich (Dorset, UK). RapidStart™ NADPH regenerating system was purchased from XenoTech (Kansas, KS, USA), William's E medium was obtained from Thermo Fisher Scientific (Paisley, UK). Human skin S9 fractions (HS-S9) was purchased from Biopredic International (Saint Grégoire, France), comprising a pooled sample prepared from the abdominal skin of 3 white female donors after plastic surgery (age range 33-46 years – *further details are provided in the supporting information*). Individual EH-TBB dosing solutions were prepared by dissolving EH-TBB in dimethyl sulfoxide (DMSO). Firemaster 550™ (FM550)-equivalent mixtures were prepared by

dissolving EH-TBB, BEH-TEBP and TPhP in the ratio 53:20.5:26.5 by weight in DMSO, similar to the reported ratio for the technical FM550 mixture (Belcher et al., 2014). Isopropyl triphenylphosphate isomers (ITP) of sufficient high purity were not available to our lab at the time of conducting this study; hence these were not included in the FM550 dosing solutions applied in the current study. FM550 solutions were prepared such that each dosing level contained concentrations of EH-TBB similar to those in the individual EH-TBB dosing solutions.

In vitro Incubation Experiments

Pre-incubations were performed at different HS-S9 concentrations and different times. After optimization of the reaction parameters, the following exposure protocol was applied: 0.11 mg of HS-S9, William's E medium and 10 µL of EH-TBB/FM550 dosing solutions (final concentration 10 µM of EH-TBB) were pre-incubated for 5 minutes at 37 ˚C. NADPH regenerating system (final concentration: 2.0 mM nicotinamide adenine dinucleotide phosphate, 10.0 mM glucose-6-phosphate and 2 units/mL glucose-6-phosphate dehydrogenase) was added to make a final volume of 1 mL. The samples were then incubated at 37 ˚C, 5% CO_2 and 98% relative humidity for 60 min. At the end of the incubation, 1 mL of ice-cold ethyl acetate was added to stop the reaction prior to sample extraction.

Sample extraction

Incubated EH-TBB samples were spiked with 20 ng each of ^{13}C-EH-TBB and ^{13}C-TBBA while FM550 samples were spiked with 20 ng each of ^{13}C-EH-TBB, ^{13}C-TBBA, ^{13}C-BEH-TEBP and TPhP-D_{15} as internal (surrogate) standards. Spiked samples were mixed with 3 mL of ethyl acetate by vortexing for 60 s, followed by ultrasonication for 5 min and

centrifuged at 4000 g for 5 min. The organic layer was collected and the extraction procedure was repeated twice. The combined extracts were evaporated to dryness under a gentle stream of nitrogen then reconstituted in 100 µL of methanol containing 20 ng of ^{13}C-α-HBCDD as a recovery determination (syringe) standard for QA/QC purposes.

Instrumental analysis

Samples were analyzed on a UPLC-Orbitrap-HRMS platform (Thermo Fisher Scientific, Bremen, Germany) composed of a Dionex Ultimate 3000 liquid chromatograph composed of a HPG-3400RS dual pump, a TCC-3000 column oven and a WPS-3000 auto sampler, coupled to a Q-Exactive Plus Orbitrap mass spectrometer. Chromatographic separation was performed on an Accucore RP-MS column (100 x 2.1 mm, 2.6 µm) with water (mobile phase A) and methanol (mobile phase B). A gradient programme at 400 µL/min flow rate was applied as follows: start at 20% B; increase to 100% B over 9 min, held for 3 min; then decrease to 20% B over 0.1 min; maintained constant for a total run time of 15 min. The mobile phase composition and gradient were selected based on the polarity and solubility of the target compounds and their reported metabolites. Methanol is used as the organic phase because none of the target compounds or their reported metabolites (e.g. monohydroxy or dihydroxy metabolites) are freely water soluble (Roberts et al., 2012; Van den Eede et al., 2013). Orbitrap-MS data from both electrospray ionization (ESI) and atmospheric pressure chemical ionization (APCI) modes was acquired for each sample. Negative APCI was used for determination of EH-TBB, ^{13}C-EH-TBB, BEH-TEBP, ^{13}C-BEH-TEBP and screening for potential metabolites. The more universal, softer ESI mode was used in positive/negative alternative switching mode for screening and identification of the produced metabolites, as well as determination of TPhP and TPhP-d_{15}. The optimized

183 Orbitrap-MS parameters for the analysis of EH-TBB, FM550 and their potential metabolites
184 are provided in Table SI-1.
185 Compound Discoverer 2.0 software (Thermo Fisher Scientific, Bremen, Germany) was used
186 to detect potential metabolites and elucidate their chemical formulae, while quantification
187 of target FRs was performed using Quan Browser 3.0 (Thermo Fisher Scientific, Bremen,
188 Germany).
189 ***QA/QC***
190 Metabolic activity of phases I enzymes including NADPH-cytochrome C reductase, carboxyl
191 esterase and FMO3 were measured using guidelines and specific kits provided by Biopredic
192 International and showed normal activities of all enzymes after HS-S9 thawing.
193 Quality assurance samples comprising William's E medium spiked with EH-TBB and
194 FM550 mixture at all dosing levels were analyzed, with recoveries of dosing chemicals
195 falling between 80 to 115% of the theoretical dosing concentrations. Internal standard
196 recoveries in all HS-S9 incubation experiments ranged from 65-115%.
197 In all incubation experiments, a solvent blank comprising William's E medium was
198 performed and analysed alongside the sample batch. No parent compounds or metabolites
199 were found in solvent blanks with the exception of TPhP at negligible levels (< 1% of the
200 lowest dosing level). Therefore, no blank correction was needed. Additionally, no
201 metabolites were found in the non-enzymatic (all experimental components except HS-S9)
202 and heat-inactivated (HS-S9 inactivated by heating at 70 °C for 30 min) controls run in
203 parallel to each sample batch.

Biotransformation kinetic modelling

The metabolite formation rate and substrate concentration of the studied chemicals were fitted to different biotransformation kinetic models (Northrop, 1983; Lipscomb and Poet, 2008) by nonlinear regression analysis using the SigmaPlot Enzyme Kinetics Module v.1.1 (Systat Software Inc., Richmond, CA) to determine the enzyme kinetic model that best describe the formation rates of the metabolites. The models used were the Michaelis-Menten equation (Equation 1), the Hill equation (Equation 2), and the substrate-inhibition kinetic equation (Equation 3) :

$$v = \frac{V_{max} \times [S]}{K_m + [S]} \qquad \text{(Equation 1)}$$

$$v = \frac{V_{max} \times [S]^n}{K' + [S]^n} \qquad \text{(Equation 2)}$$

$$v = \frac{V_{max}}{1 + \frac{K_m}{[S]} + \frac{[S]}{K_i}} \qquad \text{(Equation 3)}$$

where v is initial velocity of the reaction, Vmax is the maximum metabolic rate, [S] is the substrate concentration, Km is the Michaelis-Menten constant, K' is the Hill dissociation constant, n is the Hill coefficient and Ki is the inhibitory dissociation constant. Selection of the best fitted model was determined by statistical criteria to evaluate the goodness of the fit. The two statistical criteria used were Akaike Information Criterion corrected for small sample size (AICc) and the standard deviation of the residuals (Sy.x). The model with the lowest values for AICc and for the standard deviation of the residuals was considered to be the model that best fit the data. When the formation rate of a primary metabolite is best described by the Michaelis-Menten model (Equation 1), the part of the *in vitro* intrinsic clearance (Clint,M) due to the formation of that metabolite can be calculated as follows:

$$CL_{int,M} = \frac{v}{[S]} = \frac{V_{max}}{K_m + [S]} \qquad \text{(Equation 4)}$$

If the levels of the substrate of interest in human blood are negligible compared to the apparent Km value associated with the formation of the metabolite, then (Km + [S]) ≈ Km therefore Equation 4 can be written as follows (Lipscomb and Poet, 2008):

$$CL_{int} = \frac{v}{[S]} = \frac{V_{max}}{K_m} \quad \text{(Equation 5)}$$

The total Clint value of the substrate of interest can then be calculated as the sum of the Clint of each of its primary metabolites.

The intrinsic *in vitro* clearance of a xenobiotic by an organ on kilogram human body weight (CLint-organ) basis can be scale up by the following equation:

$$CL_{int-organ} = CL_{int} \times p \times w \quad \text{(Equation 6)}$$

Where p is the amount of protein per gram of an organ and w is the average weight of that organ per kilogram body weight.

The blood flow of an organ per kilogram body weight (kg b.w) Qh was taken into account for extrapolation of *in vitro* clearance to *in vivo* clearance (CLh) as follows (Lipscomb and Poet, 2008):

$$CL_{organ} = \frac{Q_h \times CL_{int-organ}}{CL_{int-organ} + Q_h} \quad \text{(Equation 7)}$$

Results and Discussion

Dermal metabolic profiles of EH-TBB and FM550

Due to the chemical structure of EH-TBB, BEH-TEBP and TPhP (Figure SI-1), we hypothesized that their metabolism by HS-S9 would be catalysed by carboxyesterases and/or cyctochrome P450 enzymes. Full scan mode with either APCI or alternate switching positive/negative ESI ionization were used to screen for EH-TBB and FM550 dermal

metabolites. No potential metabolites were found in (+)ESI or (-)APCI mode. For EH-TBB samples, in (-)ESI mode there was one potential metabolite with the ion mass of 436.66814 and the proposed ion formula $[C_7HBr_4O_2]^-$. By comparing with the authentic standard, this was confirmed as the $[M-H]^-$ molecular ion for TBBA (Figure 1). This is in agreement with the results of Roberts et al., who reported TBBA as the only *in vitro* metabolite of EH-TBB by human and rat liver microsomes (Roberts et al., 2012).

Following exposure of HS-S9 to FM550 mixture components, TBBA was also identified as the sole metabolite of EH-TBB. In addition, another potential metabolite with the ion mass of 249.03204 was detected in (-)ESI mode. The proposed chemical structure for this ion was $[C_{12}H_{10}O_4P]^-$. In order to elucidate the chemical structure of this compound, a MS/MS experiment was carried out in (-)ESI-SIM-MS^2 mode. A combination of low, medium and high collision energies were applied stepwise to achieve a diverse range of fragmentation ions. Specific Orbitrap-MS parameters for this experiment are provided in Table SI-2. The ion m/z = 249.03204 was fragmented mainly into three ions: 154.98895, 93.03284 and 78.95728. The proposed chemical formula for these fragments were: $[C_6H_4O_4P]^-$, $[C_6H_5O]^-$ and $[PO_3]^-$, respectively (Figure 2). Based on the proposed parent ion formula and the MS^2 fragmentation data, this metabolite was identified as diphenyl phosphate (DPhP), assigned as a primary metabolite of TPhP. Metabolite identity was further confirmed via comparison and augmentation with an authentic chemical standard of DPhP. Previous studies have reported that *in vitro* metabolism of TPhP by human liver microsomes or chicken embryo hepatocytes formed DPhP, hydroxylated TPhP (OH-TPhP) and dihydroxylated TPhP ($(OH)_2$-TPhP) (Van den Eede et al., 2013; Su et al., 2014). *In vivo* metabolism of TPhP in fish produced DPhP, OH-TPhP, $(OH)_2$-TPhP and monophenyl phosphate among which DPhP

was the major metabolite (Wang et al., 2016). However, DPhP was detected as the sole metabolite of TPhP by HS-S9 in the present study.

By comparison of the *in vitro* human dermal (this study) and hepatic metabolic profiles of EH-TBB and TPhP,(Roberts et al., 2012; Van den Eede et al., 2013) it was obvious that the oxidative metabolites could not be identified in the HS-S9 experiments under the current experimental conditions. Proteomic profiling of the metabolic activity of dermal HS-S9 fractions show that both CYP450 and carboxylesterases are active, albeit at much lower levels than in the liver cells (Oesch et al., 2018). Moreover, the reported levels of CYP450 enzymes in human skin were at least 300 fold lower than that in human liver. In contrast, the relative level of carboxylesterase 1 (CES1) in human skin and liver was 0.62 with no significant level difference (P = 0.21) (van Eijl et al., 2012). Such low level of CYP450 enzymes and similar level of CES1 in the skin in comparison with liver might explain why no oxidative metabolites were observed in the present study. To test this hypothesis, we performed NADPH-independent (i.e. without NADPH cofactor) *in vitro* incubation of EH-TBB and FM550 with HS-S9 under the same conditions. The absence of NADPH did not result in significant changes in the formation rates of TBBA, DPhP or depletion rates of the parent compounds (P>0.05). These results reveal differences from hepatic metabolism as dermal carboxylesterases seem to be the major metabolizing enzymes of the target FRs in human skin. This does not eliminate the possibility of oxidative metabolite formation upon dermal contact under real-life situations (i.e. upon exposure to larger doses) but if formed, they are likely to be at lower rates and concentrations than de-esterified metabolites.

Finally, no stable metabolites of BEH-TEBP were identified in HS-S9 exposed to FM550 mixture at any of the studied concentrations (0.3 – 4.5 μM – Table SI-2), despite the high

294 sensitivity and selectivity of the Orbitrap-MS platform applied in this study. This is in
295 agreement with the results of Roberts et al. who did not detect any metabolites for BEH-
296 TEBP in human and rat hepatic subcellular fractions. Interestingly, mono(2-ethylhexyl)
297 tetrabromophthalate, was only detected in purified hepatic porcine carboxylesterase,
298 although at a very slow formation rate of 1.08 pmol min^{-1} mg $protein^{-1}$ (Roberts et al.,
299 2012). This may reflect inter-species variation in the biotransformation of this flame
300 retardant and warrants further studies to elucidate the hepatic and extrahepatic metabolic
301 profiles of BEH-TEBP in human.

302 ***Biotransformation kinetics of EH-TBB and FM 550 by HS-S9***

303 In a previous communication, our research group reported the hepatic metabolic rates of
304 the brominated FR, 1,2-dibromo-4-(1,2 dibromoethyl) cyclohexane (TBECH), were largely
305 dependent on whether the metabolizing enzymes were challenged with a single compound
306 or a mixture of components (Nguyen et al., 2017). Therefore, a series of incubation
307 experiments of HS-S9 with different concentrations of EH-TBB and FM550 components
308 (Table SI-3) were performed. With these experiments, we aimed to investigate whether the
309 metabolic rate will be different upon challenging the HS-S9 with a multi-component
310 mixture representing FM550 (i.e. mimicking real-life situation) compared to exposure to a
311 single flame retardant (EH-TBB). The concentrations of TBBA and DPhP were quantified
312 using isotope dilution series method with ^{13}C-TBBA and d_{15}-TPhP as internal (surrogate)
313 standards. The results from kinetic modelling in SigmaPlot® software revealed the
314 formation of TBBA in both pure EH-TBB and FM550 mixture experiments was best fitted
315 by the Michaelis-Menten model (Figure 3). The model-derived kinetic parameters for the
316 formation of TBBA are presented in Table 1. Estimated maximum metabolic rate (V_{max}) for

317 the formation of TBBA upon exposure to FM550 mixture was significantly lower ($p<0.05$)
318 than V_{max} upon exposure to individual EH-TBB (1.80 and 15.2 pmol min^{-1} mg $protein^{-1}$,
319 respectively). However, in both cases, V_{max} was substantially less than that reported
320 previously for EH-TBB metabolism by human liver microsomes (644 pmol min^{-1} mg
321 $protein^{-1}$) (Roberts et al., 2012). The estimated Michaelis constant (K_m) for FM550 is lower
322 than K_m for EH-TBB metabolism by HS-S9 (Table 1). Such significant decreases in both K_m
323 and V_{max} suggest that the rate of metabolite formation (TBBA) from FM550 by HS-S9 has
324 potentially been influenced by competitive substrate inhibition. The competitive inhibitors
325 could be BEH-TEBP and/or TPhP in the FM550 dosing solutions.
326 The formation rate of DPhP (primary metabolite of TPhP) did not fit any of the assessed
327 enzyme kinetic models (Michaelis-Menten, Hill or substrate-inhibition). Indeed, it did not
328 show any signs of reaching a plateau to indicate a steady state was reached. Another series
329 of incubation experiments with higher doses of FM550 were carried out at equivalent TPhP
330 concentrations of 16.8, 25 and 33.6 µM. Close to linearity increment of DPhP formation rate
331 was still observed and steady state conditions could not be achieved. This observation is in
332 agreement with a previous study on TPhP biotransformation in human serum, where the
333 formation rate of DPhP did not reach a plateau even at concentrations up to 100 µM of
334 TPhP (Van den Eede et al., 2016). The lack of fit to the investigated kinetic models
335 precluded the estimation of metabolic kinetic parameters for TPhP under the applied
336 experimental conditions.
337 ***In vitro – in vivo extrapolation for dermal clearance of EH-TBB***
338 As the formation rates of TBBA were best described by the Michaelis-Menten model, the
339 model was applied to estimate *in vivo* dermal clearance of EH-TBB assuming average adult

bodyweight of 70 kg. We then compared our results for dermal clearance to those reported previously by Roberts et al. for human hepatic clearance of EH-TBB (Roberts et al., 2012). The following parameters were applied: 24.84 mg protein/g skin for HS-S9 (calculated as total of microsomes and cytosol),(Jewell et al., 2007) 37 g skin/kg bodyweight, 52.5 mg protein/g liver for HLM, 25.7 g liver/kg bodyweight, $\boldsymbol{Q_h}$ = 20.7 mL/min/kg bodyweight and $\boldsymbol{Q_{skin}}$ = 4.37 mL/min/kg bodyweight (Manevski et al., 2015). Our model calculations estimated *in vivo* dermal clearance of individual EH-TBB and EH-TBB in FM-550 to be 0.48 and 0.92 mL/min/kg bodyweight, respectively (Table 2). These rates were much smaller than the skin blood flow (4.37 mL/min/kg bodyweight), suggesting EH-TBB is not readily cleared by dermal metabolism and is likely to accumulate in the skin tissue. Indeed, the extraction ratios (defined as the ratio between the *in vivo* clearance of a xenobiotic to the blood flow for a specific organ)(Manevski et al., 2015) of EH-TBB by human skin were only 11% and 21% for individual and mixture exposures, respectively. This is also in agreement with the results of Frederiksen et al. (2016) who reported the accumulation of EH-TBB in the skin using a human *ex vivo* dermal model. In contrast, human liver showed higher EH-TBB extraction ratio up to 80% with *in vivo* hepatic clearance of 16.4 mL/min/kg bodyweight (Table 2). These results suggested that dermal metabolism contributed marginally to the clearance of internal EH-TBB body burden in comparison with liver metabolism.

Study limitations

It is important to note that due to limited availability, the skin HS-S9 applied in this study was pooled from the abdominal skin of 3 white female donors (age range 33-46 years). The dermal metabolic activity may vary widely depending on age, race, gender and skin

location (Oesch et al., 2018). Additionally, our *in vitro* – *in vivo* metabolic clearance calculations were based on the assumption that the unbound fraction of chemical pollutant to blood proteins equals 1, meaning all EH-TBB in the blood was free and available for metabolism. This can cause overestimation of the estimated xenobiotic clearance. Furthermore, TBBA was treated as the only primary metabolite of EH-TBB. While our experimental measurements support this assumption, it is possible that other metabolites (e.g. oxidative or debrominated metabolites) may be formed under real conditions of prolonged skin contact with high concentration of EH-TBB (e.g. sleeping on a flame retarded mattress). The potential formation of other primary metabolites under different conditions may also influence the estimated metabolic rates for EH-TBB in the current study.

Implications for human exposure

Even though the outer most layer of skin (*stratum corneum*) serves as a barrier to prevent unwanted chemicals from entering the human body, recent studies have confirmed the dermal uptake of several lipophilic pollutants such as hexabromocyclododecanes (HBCDDs), tetrabromobisphenol-A (TBBPA), organophosphate flame retardants or novel brominated flame retardants via contact with skin (Abdallah et al., 2015; Abdallah et al., 2016; Frederiksen et al., 2016; Knudsen et al., 2017). Frederiksen et al. reported roughly 10% dermal absorption and 0.1 - 0.2% penetration of several FRs including EH-TBB following a single dose (of several hundred nanograms) application to *ex vivo* human skin for 72 h (Frederiksen et al., 2016). Higher dermal uptake at 20% with 0.2% penetration of administered ^{14}C-labelled EH-TBB to *in vitro* human skin after 24 h exposure was also reported (Knudsen et al., 2016). Nevertheless, it is proven that EH-TBB as well as other

386 organic FRs can penetrate the skin barrier and be "trapped" within the skin tissue until
387 reaching the blood circulation (i.e. become bioavailable). In such an event, skin metabolism
388 may play an important role in the clearance of the trapped dose within the skin tissue, yet it
389 may also help create a concentration gradient through the different layers of the skin tissue
390 to facilitate further uptake of the parent FR. Moreover, the slow *in vitro* clearance rates in
391 the skin could translate into slow EH-TBB *in vivo* percutaneous metabolism and
392 subsequently result in inefficient removal of EH-TBB from the skin. This partially explains
393 the reported accumulation of EH-TBB in the skin tissue prior to reaching the systemic
394 circulation (Knudsen et al., 2016). In addition, very little is known about the toxicokinetics
395 and toxicodynamics of the dermal biotransformation products (i.e. TBBA and DPhP). This is
396 of concern as these metabolites may lead to potential adverse health effects similar to that
397 reported previously for PBDE metabolites (Saquib et al., 2018). Therefore, further studies
398 on dermal uptake and metabolism of emerging flame retardants are required to fully
399 understand both the toxicological and exposure implications of dermal biotransformation
400 of these hazardous chemicals.
401

402 ## Acknowledgement

403 The authors acknowledge gratefully the assistance of Mrs Adriana Carolina Torres Moreno
404 of the University of Cartagena, Colombia. This research received funding from the
405 European Union's Horizon 2020 research and innovation programme under the Marie
406 Skłodowska-Curie grant agreement No 734522 (INTERWASTE project). It also received
407 funding from the European Union Seventh Framework Programme FP7/ 2007-2013 under
408 grant agreement No. 606857 (ELUTE project).

Supporting information

Details of analytical method parameters and metabolite identification workflow are provided as supporting information.

References

Abdallah, M.A., Pawar, G., Harrad, S., 2016. Human dermal absorption of chlorinated organophosphate flame retardants; implications for human exposure. Toxicology and Applied Pharmacology 291, 28-37.

Abdallah, M.A.E., Harrad, S., 2018. Dermal contact with furniture fabrics is a significant pathway of human exposure to brominated flame retardants. Environ Int 118, 26-33.

Al-Omran, L.S., Harrad, S., 2016. Distribution pattern of legacy and "novel" brominated flame retardants in different particle size fractions of indoor dust in Birmingham, United Kingdom. Chemosphere 157, 124-131.

Belcher, S.M., Cookman, C.J., Patisaul, H.B., Stapleton, H.M., 2014. In vitro assessment of human nuclear hormone receptor activity and cytotoxicity of the flame retardant mixture FM 550 and its triarylphosphate and brominated components. Toxicology Letters 228, 93-102.

Besis, A., Christia, C., Poma, G., Covaci, A., Samara, C., 2017. Legacy and novel brominated flame retardants in interior car dust - Implications for human exposure. Environmental Pollution 230, 871-881.

Carignan, C.C., Heiger-Bernays, W., McClean, M.D., Roberts, S.C., Stapleton, H.M., Sjodin, A., Webster, T.F., 2013. Flame Retardant Exposure among Collegiate United States Gymnasts. Environmental Science & Technology 47, 13848-13856.

Cequier, E., Ionas, A.C., Covaci, A., Marce, R.M., Becher, G., Thomsen, C., 2014. Occurrence of a Broad Range of Legacy and Emerging Flame Retardants in Indoor Environments in Norway. Environmental Science & Technology 48, 6827-6835.

436 Dodson, R.E., Perovich, L.J., Covaci, A., Van den Eede, N., Ionas, A.C., Dirtu, A.C., Brody, J.G.,
437 Rudel, R.A., 2012. After the PBDE Phase-Out: A Broad Suite of Flame Retardants in Repeat
438 House Dust Samples from California. Environmental Science & Technology 46, 13056-
439 13066.
440 Frederiksen, M., Stapleton, H.M., Vorkamp, K., Webster, T.F., Jensen, N.M., Sorensen, J.A.,
441 Nielsen, F., Knudsen, L.E., Sorensen, L.S., Clausen, P.A., Nielsen, J.B., 2018. Dermal uptake
442 and percutaneous penetration of organophosphate esters in a human skin ex vivo model.
443 Chemosphere 197, 185-192.
444 Frederiksen, M., Vorkamp, K., Jensen, N.M., Sorensen, J.A., Knudsen, L.E., Sorensen, L.S.,
445 Webster, T.F., Nielsen, J.B., 2016. Dermal uptake and percutaneous penetration of ten flame
446 retardants in a human skin ex vivo model. Chemosphere 162, 308-314.
447 Hammel, S.C., Hoffman, K., Lorenzo, A.M., Chen, A., Phillips, A.L., Butt, C.M., Sosa, J.A.,
448 Webster, T.F., Stapleton, H.M., 2017. Associations between flame retardant applications in
449 furniture foam, house dust levels, and residents' serum levels. Environment International
450 107, 181-189.
451 Hopf, N.B., Berthet, A., Vernez, D., Langard, E., Spring, P., Gaudin, R., 2014. Skin permeation
452 and metabolism of di(2-ethylhexyl) phthalate (DEHP). Toxicology Letters 224, 47-53.
453 Jewell, C., Ackermann, C., Payne, N.A., Fate, G., Voorman, R., Williams, F.M., 2007. Specificity
454 of procaine and ester hydrolysis by human, minipig, and rat skin and liver. Drug
455 Metabolism and Disposition 35, 2015-2022.
456 Knudsen, G.A., Hughes, M.F., Sanders, J.M., Hall, S.M., Birnbaum, L.S., 2016. Estimation of
457 human percutaneous bioavailability for two novel brominated flame retardants, 2-
458 ethylhexyl 2,3,4,5-tetrabromobenzoate (EH-TBB) and bis(2-ethylhexyl)
459 tetrabromophthalate (BEH-TEBP). Toxicology and Applied Pharmacology 311, 117-127.
460 Lipscomb, J.C., Poet, T.S., 2008. In vitro measurements of metabolism for application in
461 pharmacokinetic modeling. Pharmacology & Therapeutics 118, 82-103.
462 Ma, Y.N., Venier, M., Hites, R.A., 2012. 2-Ethylhexyl Tetrabromobenzoate and Bis(2-
463 ethylhexyl) Tetrabromophthalate Flame Retardants in the Great Lakes Atmosphere.
464 Environmental Science & Technology 46, 204-208.
465 Manevski, N., Swart, P., Balavenkatraman, K.K., Bertschi, B., Camenisch, G., Kretz, O., Schiller,
466 H., Walles, M., Ling, B., Wettstein, R., Schaefer, D.J., Itin, P., Ashton-Chess, J., Pognan, F., Wolf,

A., Litherland, K., 2015. Phase II Metabolism in Human Skin: Skin Explants Show Full Coverage for Glucuronidation, Sulfation, N-Acetylation, Catechol Methylation, and Glutathione Conjugation. Drug Metabolism and Disposition 43, 126-139.

Mankidy, R., Ranjan, B., Honaramooz, A., Giesy, J.P., 2014. Effects of novel brominated flame retardants on steroidogenesis in primary porcine testicular cells. Toxicology Letters 224, 141-146.

Nguyen, K.H., Abdallah, M.A.E., Moehring, T., Harrad, S., 2017. Biotransformation of the Flame Retardant 1,2-Dibromo-4-(1,2-dibromoethyl)cyclohexane (TBECH) in Vitro by Human Liver Microsomes. Environmental Science & Technology 51, 10511-10518.

Northrop, D.B., 1983. FITTING ENZYME-KINETIC DATA TO V/K. Anal. Biochem. 132, 457-461.

Oesch, F., Fabian, E., Landsiedel, R., 2018. Xenobiotica-metabolizing enzymes in the skin of rat, mouse, pig, guinea pig, man, and in human skin models. Archives of Toxicology 92, 2411-2456.

Patisaul, H.B., Roberts, S.C., Mabrey, N., McCaffrey, K.A., Gear, R.B., Braun, J., Belcher, S.M., Stapleton, H.M., 2013. Accumulation and Endocrine Disrupting Effects of the Flame Retardant Mixture Firemaster (R) 550 in Rats: An Exploratory Assessment. Journal of Biochemical and Molecular Toxicology 27, 124-136.

Pillai, H.K., Fang, M.L., Beglov, D., Kozakov, D., Vajda, S., Stapleton, H.M., Webster, T.F., Schlezinger, J.J., 2014. Ligand Binding and Activation of PPAR gamma by Firemaster (R) 550: Effects on Adipogenesis and Osteogenesis in Vitro. Environmental Health Perspectives 122, 1225-1232.

Roberts, S.C., Macaulay, L.J., Stapleton, H.M., 2012. In Vitro Metabolism of the Brominated Flame Retardants 2-Ethylhexyl-2,3,4,5-Tetrabromobenzoate (TBB) and Bis(2-ethylhexyl) 2,3,4,5-Tetrabromophthalate (TBPH) in Human and Rat Tissues. Chemical Research in Toxicology 25, 1435-1441.

Saquib, Q., Siddiqui, M.A., Ahmad, J., Ansari, S.M., Al-Wathnani, H.A., Rensing, C., 2018. 6-OHBDE-47 induces transcriptomic alterations of CYP1A1, XRCC2, HSPA1A, EGR1 genes and trigger apoptosis in HepG2 cells. Toxicology 400, 40-47.

Saunders, D.M.V., Higley, E.B., Hecker, M., Mankidy, R., Giesy, J.P., 2013. In vitro endocrine disruption and TCDD-like effects of three novel brominated flame retardants: TBPH, TBB, & TBCO. Toxicology Letters 223, 252-259.

Strid, A., Bruhn, C., Sverko, E., Svavarsson, J., Tomy, G., Bergman, A., 2013. Brominated and chlorinated flame retardants in liver of Greenland shark (Somniosus microcephalus). Chemosphere 91, 222-228.

Stubbings, W.A., Schreder, E.D., Thomas, M.B., Romanak, K., Venier, M., Salamova, A., 2018. Exposure to brominated and organophosphate ester flame retardants in US childcare environments: Effect of removal of flame-retarded nap mats on indoor levels. Environmental Pollution 238, 1056-1068.

Su, G.Y., Crump, D., Letcher, R.J., Kennedy, S.W., 2014. Rapid in Vitro Metabolism of the Flame Retardant Triphenyl Phosphate and Effects on Cytotoxicity and mRNA Expression in Chicken Embryonic Hepatocytes. Environmental Science & Technology 48, 13511-13519.

Tao, F., Abdallah, M.A., Ashworth, D.C., Douglas, P., Toledano, M.B., Harrad, S., 2017. Emerging and legacy flame retardants in UK human milk and food suggest slow response to restrictions on use of PBDEs and HBCDD. Environment International 105, 95-104.

Tao, F., Abdallah, M.A.E., Harrad, S., 2016. Emerging and Legacy Flame Retardants in UK Indoor Air and Dust: Evidence for Replacement of PBDEs by Emerging Flame Retardants? Environmental Science & Technology 50, 13052-13061.

Van den Eede, N., Ballesteros-Gomez, A., Neels, H., Covaci, A., 2016. Does Biotransformation of Aryl Phosphate Flame Retardants in Blood Cast a New Perspective on Their Debated Biomarkers? Environmental Science & Technology 50, 12439-12445.

Van den Eede, N., Maho, W., Erratico, C., Neels, H., Covaci, A., 2013. First insights in the metabolism of phosphate flame retardants and plasticizers using human liver fractions. Toxicology Letters 223, 9-15.

van Eijl, S., Zhu, Z.Y., Cupitt, J., Gierula, M., Gotz, C., Fritsche, E., Edwards, R.J., 2012. Elucidation of Xenobiotic Metabolism Pathways in Human Skin and Human Skin Models by Proteomic Profiling. Plos One 7.

Wang, G.W., Du, Z.K., Chen, H.Y., Su, Y., Gao, S.X., Mao, L., 2016. Tissue-Specific Accumulation, Depuration, and Transformation of Triphenyl Phosphate (TPHP) in Adult Zebrafish (Danio rerio). Environmental Science & Technology 50, 13555-13564.

Xu, F.C., Garcia-Bermejo, A., Malarvannan, G., Gomara, B., Neels, H., Covaci, A., 2015. Multi-contaminant analysis of organophosphate and halogenated flame retardants in food matrices using ultrasonication and vacuum assisted extraction, multi-stage cleanup and gas chromatography-mass spectrometry. Journal of Chromatography A 1401, 33-41.

Zheng, X.B., Xu, F.C., Luo, X.J., Mai, B.X., Covaci, A., 2016. Phosphate flame retardants and novel brominated flame retardants in home-produced eggs from an e-waste recycling region in China. Chemosphere 150, 545-550.

Tables

Table 1: Kinetic parameters derived from Michaelis-Menten model for the formation of TBBA following incubation of HS-S9 with pure EH-TBB and FM550 mixture in the present study compared to the reported parameters for EH-TBB incubation with human liver microsomes (HLM).(Roberts et al., 2012)

Substrate	Model	K_m (µM) ± standard deviation	V_{max} (pmol/min/mg protein) ± standard deviation
EH-TBB	HS-S9	4.57 ± 1.2	15.2 ± 5
FM550	HS-S9	0.84 ± 0.19	1.80 ± 0.05
EH-TBB	HLM	11.1 ± 3.9	644 ± 144

Table 2: Estimated *in vitro* and *in vivo* clearance of EH-TBB by human skin (the current study) compared to those reported in human liver (Roberts et al., 2012).

Chemical	Organ	$CL_{int\text{-}organ}$ (*in vitro*, mL/min/kg b.w)	CL_{organ} (*in vivo*, mL/min/kg b.w)
EH-TBB	Skin	0.54	0.48
EH-TBB in FM550	Skin	1.18	0.92
EH-TBB	Liver	78.3	16.4

Figures

Figure 1: TBBA detected as the sole metabolite of EH-TBB in Human Skin S9 fraction (HS-S9) exposed to 10 µM of EH-TBB. ^{13}C-TBBA is the isotope-labelled form used for identity confirmation and quantification of TBBA.

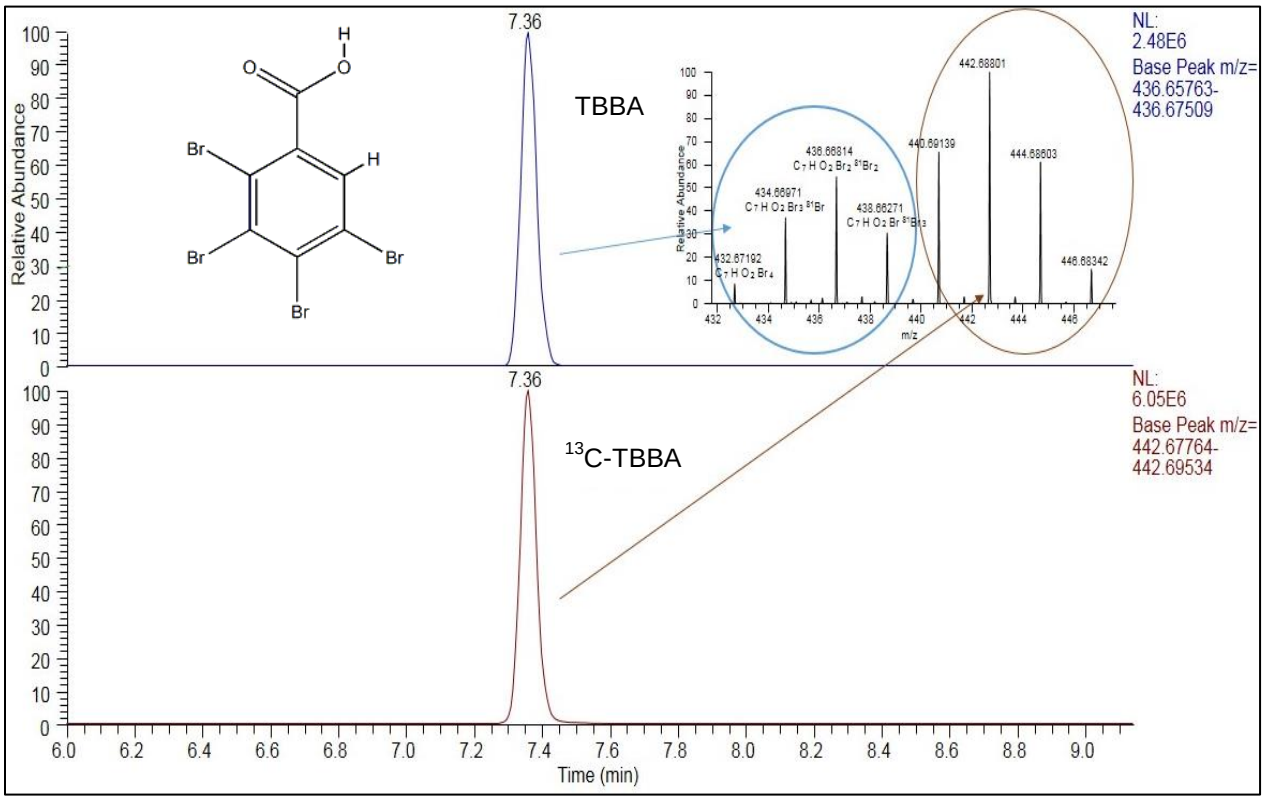

584 Figure 2: (-)ESI-MS/MS² spectrum of the ion 249.03204 by UPLC-Orbitrap HRMS

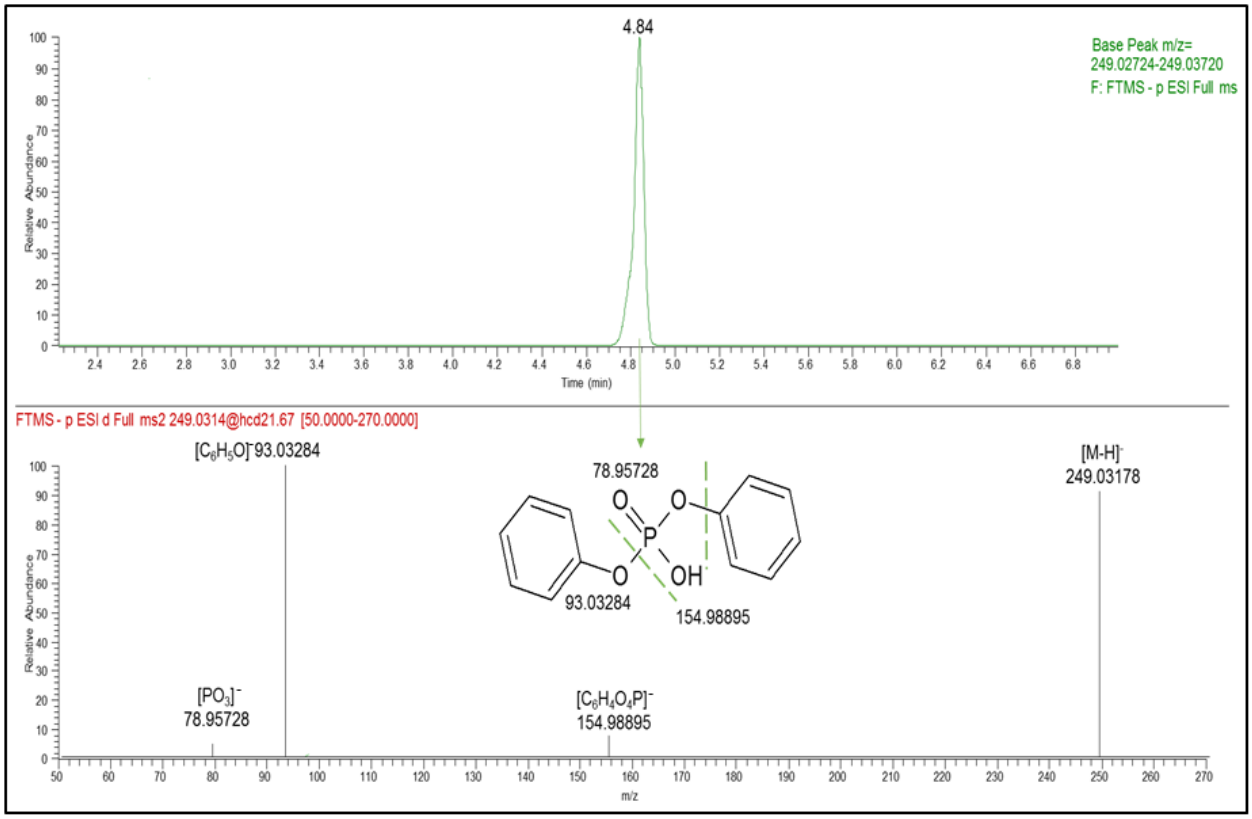

585

586

587

588

589

590

591

592

593

594

595

596

Figure 3: Kinetics of TBBA formation in EH-TBB (A) and FM550 mixture (B) incubation experiments with HS-S9 using the Michaelis-Menten model. Error bars represent 1 standard deviation (n=3).